Published in final edited form as:
Bioorg Med Chem. 2012 April 1; 20(7): 2435–2443. doi:10.1016/j.bmc.2012.01.037.

Intramolecular Hydrogen Bonding: A Potential Strategy for More Bioavailable Inhibitors of Neuronal Nitric Oxide Synthase

Kristin Jansen Labby[1], **Fengtian Xue**[1,†], **James M. Kraus**[1], **Haitao Ji**[1,§], **Jan Mataka**[1], **Huiying Li**[2], **Pavel Martásek**[3,4], **Linda J. Roman**[3], **Thomas L. Poulos**[2,*], and **Richard B. Silverman**[1,*]

[1]Department of Chemistry, Department of Molecular Biosciences, Center for Molecular Innovation and Drug Discovery, Northwestern University, 2145 Sheridan Road, Evanston, Illinois 60208-3113

[2]Departments of Molecular Biology and Biochemistry, Chemistry, and Pharmaceutical Sciences, University of California, Irvine, Irvine, California, 92697-3900

[3]Department of Biochemistry, University of Texas Health Science Center, San Antonio, Texas

[4]Department of Pediatrics, 1st School of Medicine, Charles University, Prague, Czech Republic

Abstract

Selective neuronal nitric oxide synthase (nNOS) inhibitors have therapeutic applications in the treatment of numerous neurodegenerative diseases. Here we report the synthesis and evaluation of a series of inhibitors designed to have increased cell membrane permeability via intramolecular hydrogen bonding. Their potencies were examined in both purified enzyme and cell-based assays; a comparison of these results demonstrates that two of the new inhibitors display significantly increased membrane permeability over previous analogs. NMR spectroscopy provides evidence of intramolecular hydrogen bonding under physiological conditions in two of the inhibitors. Crystal structures of the inhibitors in the nNOS active site confirm the predicted non-intramolecular hydrogen bonded binding mode. Intramolecular hydrogen bonding may be an effective approach for increasing cell membrane permeability without affecting target protein binding.

Keywords

neuronal nitric oxide synthase; enzyme inhibitors; intramolecular hydrogen bond

*Correspondence to Prof. Richard B. Silverman at the Department of Chemistry Agman@chem.northwestern.edu; phone: +1 847-491-5653; fax: +1 847-491-7713. Prof. Thomas L. Poulos, poulos@uci.edu; 949-824-7020.
†Current Address: Department of Pharmaceutical Sciences, University of Maryland School of Pharmacy, 20 North Pine Street, Baltimore, Maryland, 21201
§Current address: Department of Chemistry, University of Utah, Salt Lake City, UT 84112

PDB accession codes: The PDB accession codes for compounds **4a–d** with nNOS, shown in Figure 3 are as follows: nNOS-**4a**, 3TYL; nNOS-**4b**, 3TYM; nNOS-**4c**, 3TYN; nNOS-**4d**, 3TYO.

Supplementary data
Supplementary data associated with this article can be found in the online version of the article. These data include full ^{1}H and ^{13}C NMR spectra of **4a–4d**.

1. Introduction

Neurodegeneration, characterized by progressive loss of neurons in isolated areas of the central nervous system (CNS), has become a rapidly spreading health crisis in the world. It affects the lives of millions of people, causing problems with motor skills and memory. Although significant research advances have been made, effective treatments for neurodegenerative disorders have remained elusive. An abnormally high concentration of cerebral nitric oxide (NO), the metabolite of the neuronal isoform of nitric oxide synthases (nNOS), has been observed as a common pathogenic phenomenon shared by various neurodegenerative conditions, including Alzheimer's, [1] Parkinson's, [2] Huntington's,[3] migraine headaches,[4] as well as neuronal damage in stroke.[5] High NO concentrations provide a rationale for the therapeutic use of nNOS inhibitors as a potential simultaneous treatment for different types of neurodegeneration. In the past two decades, a large number of nNOS inhibitors have been reported.[6–9,9] However, none of these compounds has been approved for medical use. Recently, we reported a family of *syn*-3,4-substituted pyrrolidine inhibitors (e.g., **1**–**3**, Figure 1) that were discovered using structure-based drug design.[10–13] These inhibitors showed remarkable potency for nNOS and excellent isoform selectivity over endothelial NOS (eNOS) and inducible NOS (iNOS).We have previously found that the (3*S*,4*S*)-isomers of **1** and **3** bind to nNOS in the predicted mode with the 3-fluorophenyl group bound in the hydrophobic cleft comprised of M336 and L337 and the aminopyridine interacting with E592, but unexpectedly the (3*R*,4*R*)-isomers bind with 180° rotation with the 3-fluorophenyl group -stacked over the active site heme and the aminopyridine electrostatically interacting with a carboxylate of heme propionate.[11] Also surprising, the (3*R*,4*R*)-isomers are more potent than the (3*S*,4*S*)-isomers. However, results from animal tests indicated that racemic mixtures of **1** and **3** (and their corresponding 3*R*,4*R* stereoisomers) show minimal blood-brain barrier (BBB) penetration;[13] the BBB is a unique barrier formed by brain capillary endothelial cells that molecules must be able to penetrate to be effective in the CNS. This result limits further investigation of these lead compounds as oral therapeutics. Given the chemical structures of the inhibitors, we reasoned that the multiple positive charges and hydrogen bond donor properties of **1**–**3** at physiological pH, derived from the amino groups, limit them from penetrating the BBB by passive diffusion.[13] Lead compound **3**was designed to eliminate one of the hydrogen bond donors of **1**, the amino group attached to the pyrrolidine ring, by replacing it with a hydrogen bond acceptor ether linkage; hydrogen bond donors are believed to lower the ability to cross the BBB more than hydrogen bond acceptors. Supporting our rationale, BBB penetration was slightly improved from the design of **1** to **3**, but there is still much room for improvement in the bioavailability of these selective inhibitors.[13]

In previous efforts we pursued different strategies to modify the structure of compounds in this class.[13–17] For example, the high pK_a amino groups have been replaced by neutral functionalities such as ethers and amides.[13] We have also inserted electron-withdrawing groups, such as ether, monofluoromethylene, difluoromethylene, and cyclopropyl, to inductively decrease the pK_a of the amino group.[14–17] Despite the improved membrane permeability of the new inhibitors, the successes of these modified structures were compromised by a significant drop in the *in vitro* potency and isoform selectivity.

Here we describe the design and synthesis of a new series of nNOS inhibitors (**4a**–**d**, Figure 2) to diffuse the overall charge of **3** by incorporation of an intramolecular hydrogen bond, a known strategy in the design of novel inhibitors for a variety of enzymes, [18–23] sometimes used to improve BBB penetration.[24] In the highly hydrophobic environment of the BBB, the inhibitor is hypothesized to adopt a "closed" conformation by forming an intramolecular H-bond, which decreases the overall polarity of the compound to improve BBB permeability. On the other hand, when the inhibitor reaches and binds to nNOS, it may

encounter various intermolecular interactions and stabilize an "open" (not intramolecular hydrogen bonded) conformation. In this conformation, the pharmacologically critical amino group may be released from the intramolecular H-bond. Compounds **4a–d** have benzyl-like aryl substituents like **2**[25] rather than phenylethyl-like aryl substituents like **1**[26] and **3**, [26] so that 6-membered instead of 7-membered intramolecular hydrogen bonds would form. Therefore, we chose to make the (3*S*,4*S*)-isomers that bind in the normal mode, despite the generally lower potency in the phenylethyl series; computer modeling suggested that with a one-carbon shorter side chain compounds would have better binding, although the (3*R*,4*R*) compounds have not been made to confirm. Six-membered intramolecular H-bonds are most common, the majority of which are linked by sp^2-hybridized atoms and are therefore part of planar conjugated systems; five-membered intramolecular hydrogen bonds also have precedence.[18]

2. Chemistry

The synthesis of inhibitors **4a**–**d** began with chiral precursor **5**.[27] Allylation of **5** using gave alkene **6** in good yields.[28] Ozonolysis allyl methyl carbonate in the presence of $Pd(PPh_3)_4$ of **6** yielded aldehyde **7**, which was subjected to reductive amination with amines to provide **8a**–**d**. Global deprotection of the three Boc-protecting groups with TFA generated inhibitors **4a**–**d** in quantitative yields.

3. Results and Discussion

3.1 Assay with purified nNOS

The potencies of these compounds have been tested both in a purified enzyme assay and in a cell-based assay. The purified enzyme assay results demonstrate that **4a–d** have lower potencies for nNOS and lower selectivities over eNOS and iNOS in comparison with our previous inhibitors **1**–**3** (Table 1), [25,26] but compounds **4a–d** are proof-of-principle compounds to test their ability to permeate a cell membrane.

3.2 Assay in HEK293t cells

We have employed a simple, colorimetric, cell-based assay using HEK293t cells stably transfected with and expressing nNOS to assess the potencies of these compounds in a cellular environment. [29] Although other processes may be influencing nNOS inhibition in these assays, cell permeability can be predicted from the cellular potencies of these compounds as measured by the inhibition of the production of nitric oxide in the HEK293t cells (Table 2). Comparing the IC_{50} values of these compounds in the purified enzyme assay versus the cellular assay clearly indicates that membrane permeability is a major factor that limits the effective concentration of these inhibitors within cells. Therefore, the Relative Permeability Index (RPI) is a measure of how similar the IC_{50} value is for a compound as measured in the cell-based assay relative to the purified enzyme assay. If a compound freely passed through the cell membrane, then those IC_{50} values should be the same (cell based IC_{50}/purified enzyme IC_{50} = 1.0). The lower the RPI, the more cell membrane-penetrable is the compound. Therefore, **4a** and **4b** have the highest cell penetrability compared to **1**–**3**, and **4c** is comparable in penetrability relative to **3**, despite the poorer inhibitory properties of these compounds relative to **1**–**3**. As depicted in Figure 2, however, **4c** had the greatest theoretical potential to neutralize the charge on the ammonium ion, yet it did not exhibit high cell permeability. That may suggest that the phenolic hydroxyl group does not act as a hydrogen bond donor. Compound **4d**, with the highest IC_{50} of all compounds in the table, is nonetheless more cell-penetrable than **1** and **2**. We also tested just the aminopyridine fragment of inhibitors **1**–**4** (2-amino-4,6-dimethylpyridine hydrochloride), which is a potent, nonselective inhibitor of purified nNOS (50 nM); however, its RPI is much higher than any

of our inhibitors, indicating that it poorly crosses the cell membrane despite having a neutral pK_a. Although L-*N*-nitroarginine (L-NNA) is a relatively poor inhibitor of purified nNOS, it appears to penetrate the cell membrane freely, having the same IC_{50} value in the cell-based assay as the isolated enzyme assay and a RPI of **1**.

It is interesting to note that the relative permeability index has little correlation with partition coefficients for the inhibitors. As calculated by Chem Axon [30], the cLogP values are as follows: 2.18 (**1**); 2.35 (**2)**; 2.49(**3)**; 2.2 (**4a)**; 1.9 (**4b)**; −0.09 (**4c)**; 1.12 (**4d)**. For this series, cLogP seems to be a poor predictor of permeability as measured by the NOS cell-based assay.

3.3 Crystallography of 4a–d bound to nNOS

Crystal structures of all four compounds bound to nNOS were obtained, showing that when bound to nNOS, they all adopt the open, non-intramolecular hydrogen bonded form (Figure 3). Inhibitors **4a–4d** (like **1**–**3)**, bear a (3*S*,4*S*) configuration at the pyrrolidine ring, and all bind to the nNOS active site in the normal binding mode, with the 2-amino-4-methylpyridine stacked over the heme plane and hydrogen bonding with Glu592.[11] The pyrrolidine nitrogen hydrogen bonds with Glu592 and interacts through a water-bridged hydrogen bond with Asp597, the residue that can be exploited for selectivity between nNOS and eNOS (Asn368 in eNOS). The amino group that was designed to form an intramolecular hydrogen bond with the substituent from the tail aromatic ring is exposed in the crystal structures and hydrogen bonds with heme propionate D in all four inhibitors. Compounds **4a–c** have a substituted phenyl tail, but **4d** contains a furan in place of the phenyl ring. The substituted phenyls and the furan ring occupy the pocket lined with hydrophobic residues Met336, Leu337, and Tyr706. The furan is smaller than the phenyl substituents, so it is able to accommodate a different rotamer of Met336 in which it rotates in toward the inhibitor molecule. The slightly higher K_i of **4b**, the methoxyl-substituted inhibitor, may result from a slight steric clash with Trp306 (subunit B) in this pocket.

Figure 3B shows a comparison of the binding mode of **4a–d** with that of previously designed (3*S,*4*S*) inhibitors **1**–**3** using an overlay of **1** and **3** with **4a**. Inhibitor **1** (**2** as well) contains a nitrogen atom in place of the oxygen atom adjacent to the pyrrolidine in **3** and **4a–d**. It is this amino nitrogen in **1** (and **2**) that makes a hydrogen bond with a different heme propionate (of pyrrole A). The ether oxygen in **3** and **4a–d** does not have a proton to make this hydrogen bond. Instead, **3** and **4a–d** all curl so that the other amino group next to the aromatic tail group can hydrogen bond with heme propionate D. The inhibitors with an amine next to the pyrrolidine (**1** and **2**), generally bind tighter to nNOS (Figure 1) than the ones bearing an ether oxygen at the same position (**3** and **4a–d,** Table 1). However, the ether inhibitors show better bioavailability.[14,17] Another noticeable difference in the crystal structure between inhibitors **1** and **3** and series **4a–d** occurs because of one less carbon unit in the chain to the phenyl substituent in the latter. The hydrophobic pocket is large enough to accommodate either chain length. However, the inhibitors with a longer chain length make tighter van der Waals contacts with Met336, Leu337, and Tyr706, thus showing better binding affinity than the shorter tailed **4a–d**. Inhibitor **2** has the same chain length as **4a–d** but **2** has better binding affinity than **4a–d**. This is because the amino group next to the pyrrolidine in **2** hydrogen bonds to heme propionate A, so that the rest of its fluorophenyl tail adopts an extended conformation rather the curled one seen in **4a–d**, allowing tighter hydrophobic interactions with the surrounding protein.

3.4 NMR spectroscopy to determine extent of hydrogen bonding

Inspection of the ^{1}H NMR spectra of these compounds in D_2O at room temperature shows a striking difference in the splitting pattern of the methylene group (4.2 ppm) in the

arylalkylside chain (Figure 4). When the intramolecular H-bond forms, the interaction of the phenyl ortho-substituent differentiates the two protons of the ammonium and makes the ammonium nitrogen chiral. This anisotropy [32,34] is evident as a second-order effect in the ^{1}H NMR spectrum because the side chain methylene protons are diastereotopic. In the ^{1}H NMR spectra of **4b** and **4c,** these protons exhibit an AB pattern, two separate but coupled doublets, instead of the singlet expected for these identical protons. The average shift of the AB quartet is centered at the chemical shift of the expected singlet, and the doublets for the individual protons are found shifted upfield or downfield.

In contrast, the observed signal in the NMR spectra for the methylene protons of **4a** and **4d** (Figure 4) is the expected singlet at approximately 4.2 ppm. In these two compounds the methylene protons are also diastereotopic (as in **4b** and **4c**), but the lack of a stable interaction to differentiate the protons of the ammonium gives rise to a singlet for the methylene protons. Therefore, there is likely no significant intramolecular hydrogen bonding interaction occurring in these compounds at room temperature in an aqueous environment, and more importantly, not under physiological conditions (37 °C). Fluorine-mediated hydrogen bonds are weak (if observable at all), and these results (**4a**) are consistent with this observation. A five-membered intramolecular hydrogen bond (**4d**) is known to be the least likely to form.[18]

An examination of the NMR spectra of **4b** and **4c** in D_2O at various temperatures provides further evidence of the hydrogen bond character. The two doublets shift at higher temperatures, as seen in Figure 5. Unfortunately the doublets of **4b** are slightly obscured by the shift of the pyrrolidine proton (at 25 °C, 4.12 ppm) and spectral resolution decreases at 95 °C; nonetheless, Figure 5 illustrates that the chemical shifts of the doublets are moving closer together as the temperature increases. In both inhibitors, hydrogen bonding is observed in water at physiological pH, and the temperature at which doublets would be expected to collapse into a singlet is well above the physiological temperature of 37 °C. This suggests that the intramolecular hydrogen bonds of **4b** and **4c** are stable in solution at high temperatures and that this approach would be amenable to enhancing membrane permeability in vivo.

Interestingly, **4a** and **4b** demonstrate the highest relative permeability (Table 2), although it is **4b** and **4c** that display NMR spectral evidence of a H-bond. The o-fluorophenyl group of permeable inhibitor **4a** is the most lipophilic side chain group of the series and also the most electron withdrawing; the increased electron withdrawing character lowers the pK_a of the ammonium group, making it less basic. Both of these properties might account for the enhanced permeability of **4a**. This is consistent with the findings of Ballet et al. who concluded that lipophilicity rather than side chain flexibility is the key determinant for BBB penetration.[35] Compound **4c**, despite its ability to intramolecular hydrogen bond has a polar phenolic hydroxyl group, which would hinder cell permeability.

4. Conclusion

New nNOS inhibitors **4a**–**d** have been synthesized derived from chiral pyrrolidine lead **2**. Crystal structures confirm that these compounds bind to nNOS in the “open” conformation, while ^{1}H NMR spectra provide evidence of intramolecular hydrogen bonding, the “closed” conformation, in two of the compounds (**4b** and **4c**). It appears, however, that incorporation of an intramolecular hydrogen bond is not sufficient to enhance cell membrane permeability; lipophilicity seems to play a larger role, as evidenced by the good permeability of **4a** and the poor permeability of **4c**. Inhibitors **4a** and **4b** demonstrate greatly improved cell permeability when compared to previous inhibitors **1**–**3**. For inhibitor **4b,** its improved permeability likely results from intramolecular hydrogen bonding to diffuse the positive

charge on the vicinal ammonium ion. Once the compounds enter the active site of nNOS, however, intermolecular binding interactions overcome the intramolecular hydrogen bonds, resulting in the predicted open-conformation binding mode. This suggests that intramolecular hydrogen bonding can accomplish the desired decreased polarity for enhanced cell membrane permeability, but not interfere with desired binding interactions in the target protein. The purpose of these studies was to demonstrate the effect of hydrogen bonding on cell permeability; the next step in the process will be to modify the compounds for better binding potency without loss of cell membrane permeability.

5. Experimental Section

5. 1 General Methods

All experiments were conducted under anhydrous conditions in an atmosphere of argon, using flame-dried apparatus and employing standard techniques in handling air-sensitive materials. All solvents were distilled and stored under an argon or nitrogen atmosphere before using. All reagents were used as received. Aqueous solutions of sodium bicarbonate, sodium chloride (brine), and ammonium chloride were saturated. Analytical thin layer chromatography was visualized by ultraviolet light. Flash column chromatography was carried out under a positive pressure of nitrogen. ^{1}H NMR spectra were recorded on 500 MHz spectrometers. Data are presented as follows: chemical shift (in ppm on the δ scale relative to δ = 0.00 ppm for the protons in tetramethylsilane (TMS)), integration, multiplicity (s = singlet, d = doublet, t = triplet, q = quartet, m = multiplet, br = broad), coupling constant (*J*/Hz). Coupling constants were taken directly from the spectra and are uncorrected. ^{13}C NMR spectra were recorded at 125 MHz, and all chemical shift values are reported in ppm on the δ scale with an internal reference of δ 77.0 or 49.0 for $CDCl_3$ or MeOD, respectively. High-resolution mass spectra were measured by liquid chromatography/time-of-flight mass spectrometry (LC-TOF). The purity of the final compounds was determined by HPLC analysis to be ≥95%. The column used was a Higgins Analytical, TARGA®C18, 5 μm, 4.6 × 250 mm (p/n: TS-2546-C185, The Nest Group, Inc., http://www.nestgrp.com). The column was thoroughly equilibrated at 100% solvent A, minimum 5 volumes. The compounds were eluted with a gradient from solvent A (water, 0.1% TFA) to solvent B (acetonitrile, 0.1% TFA), 0–5 minutes, 0–25% B, 5–10, 25–35% B, 10–20 35% isocratic. The compounds had the following retention times, **4a**, 11.2 min, **4b**, 11.6 min, **4c**, 11.4 min, **4d**, 10.5 min.

5.2 Preparation and Characterization of New Compounds

5.2.1 (3*S*,4*S*)-*tert*-Butyl-3-(allyloxy)-4-((6-(bis(*tert*-butoxycarbonyl)amino)-4-methylpyridin-2-yl)methyl)pyrrolidine-1-carboxylate (6)—To a solution of **5** (1.15 g, 2.0 mmol) and $Pd(Ph_3P)_4$ (235 mg, 0.2 mmol) in dry THF (50 mL) was added allyl methyl carbonate (700 μL, 6.0 mmol). The reaction mixture was allowed to stir at 45 °C for 5 h and then concentrated. The resulting material was purified by flash column chromatography (silica gel, EtOAc/hexanes, 1:2, R_f = 0.40) to yield **6** (675 mg, 66%) as a colorless oil: ^{1}H NMR (500 MHz, $CDCl_3$) 1.40–1.50 (m, 27H), 2.25–2.27 (m, 3H), 2.60–2.75 (m, 1H), 2.78–2.85 (dd, *J* = 9.0, 13.5 Hz, 1H), 2.98–3.05 (dd, *J* = 9.0, 13.5 Hz, 1H), 3.10–3.21 (m, 1H), 3.25–3.29 (dd, *J* = 4.0, 12.5 Hz, 1H), 3.40–3.62 (m, 2H), 3.75–3.85 (m, 2H), 4.00–4.10 (td, *J* = 5.5, 13.0 Hz, 1H), 5.15–5.17 (d, *J* = 10.5 Hz, 1H), 5.25–5.29 (d, *J* = 17.0 Hz, 1H), 5.84–5.91 (ddd, *J* = 5.0, 10.5, 17.0 Hz, 1H), 6.85–6.95 (m, 2H); ^{13}C NMR (125 MHz, $CDCl_3$) 20.9, 27.9, 28.4, 28.5, 34.7, 34.8, 42.7, 43.3, 48.9, 49.2, 50.4, 51.0, 70.2, 70.3, 77.8, 78.6, 79.1, 79.2, 82.8, 116.7, 116.9, 119.6, 122.9, 134.6, 134.7, 149.50, 149.52, 151.4, 151.5, 151.8, 154.5, 154.8, 159.2, 159.3; LC-TOF ($M+H^+$) calcd for $C_{29}H_{46}N_3O_7$ 548.3336, found 548.3339.

5.2.2 (3*S*,4*S*)-*tert*-Butyl-3-((6-(bis(*tert*-butoxycarbonyl)amino)-4-methylpyridin-2-yl)methyl)-4-(2-oxoethoxy)pyrrolidine-1-carboxylate (7)—A solution of **6** (100 mg, 0.19 mmol) in CH_2Cl_2 (10 mL) was cooled to −78 °C, to which O_3 was charged until the reaction solution turned purple (~10 min). The O_3 flow was stopped, and the reaction was allowed to stir at the same temperature for 30 min. To the resulting solution was added Me_2S (150 μL). The reaction mixture was then warmed to room temperature and kept stirring at room temperature for an additional 2 h. The solvent was removed by rotary evaporation and the resulting crude product was purified by flash column chromatography (EtOAc/hexanes, 1:1, R_f = 0.2) to yield **6** (87 mg, 87%) as a colorless oil: ^{1}H NMR (500 MHz, $CDCl_3$) 1.45 (s, 27H), 2.22 (s, 3H), 2.70–2.85 (m, 1H), 2.85–2.95 (m, 1H), 3.05–3.15 (m, 1H), 3.16–3.25 (m, 1H), 3.30–3.37 (m, 1H), 3.45–3.70 (m, 2H), 3.85–3.95 (m, 2H), 4.05–4.20 (t, *J* = 10.0 Hz, 1H), 6.90–6.93 (m, 2H), 9.66 (s, 1H); ^{13}C NMR (125 MHz, $CDCl_3$) 20.9, 24.7, 27.9, 28.5, 29.7, 34.4, 42.5, 43.2, 48.8, 49.1, 50.3, 51.0, 74.6, 74.9, 79.4, 79.5, 80.4, 83.0, 119.66, 119.73, 122.8, 149.7, 149.8, 151.57, 151.60, 151.8, 154.4, 154.8, 159.87, 158.94, 200.2, 200.6; LC-TOF ($M+H^+$) calcd for $C_{28}H_{44}N_3O_8$ 550.3128, found 550.3130.

5.2.3 (3*S*,4*S*)-*tert*-Butyl-3-((6-(bis(*tert*-butoxycarbonyl)amino)-4-methylpyridin-2-yl)methyl)-4-(2-(2-fluorobenzylamino)ethoxy)pyrrolidine-1-carboxylate (8a)—To a solution of aldehyde **7** (100 mg, 0.18 mmol) in DCM (4 mL) was added 2,2-difluoro-2-(3-fluorophenyl)ethanamine hydrochloride (83 mg, 0.36 mmol), triethylamine (11 μL, 0.36 mmol), followed by $NaHB(OAc)_3$ (100 mg, 0.45 mmol). The reaction mixture was stirred for an additional 3 h and then concentrated. The crude product was purified by flash column chromatography (EtOAc/hexanes, 1:1, R_f = 0.15) to yield **8a** (115 mg, 91%) as a colorless oil: ^{1}H NMR (500 MHz, $CDCl_3$) 1.43–1.44 (s, 27H), 2.29–2.30 (m, 3H), 2.60–2.75 (m, 1H), 2.76–2.85 (m, 2H), 2.92–3.00 (m, 1H), 3.05–3.14 (m, 1H), 3.20–3.50 (m, 5H), 3.52–3.70 (m, 2H), 3.72–3.80 (m, 1H), 3.91 (s, 2H), 6.84–6.85 (d, *J* = 8.0 Hz, 1H), 6.89–6.91 (d, *J* = 10.0 Hz, 1H), 7.02–7.06 (dd, *J* = 9.0, 9.5 Hz, 1H), 7.10–7.13 (dd, *J* = 7.0, 7.5 Hz, 1H), 7.20–7.30 (m, 1H), 7.35–7.40 (m, 1H); ^{13}C NMR (125 MHz, $CDCl_3$) 20.9, 24.7, 27.9, 28.47, 28.50, 29.7, 34.6, 34.7, 36.6, 42.6, 43.3, 46.8, 48.2, 48.8, 49.1, 50.3, 50.8, 68.0, 68.2, 78.7, 79.2, 79.3, 79.4, 82.8, 115.2, 115.3, 115.4, 115.5, 119.5, 119.6, 122.8, 124.17, 124.19, 128.89, 128.92, 128.95, 128.99, 130.46, 130.51, 130.55, 149.6, 151.4, 151.5, 151.8, 154.5, 154.8, 159.08, 159.14, 160.3, 162.2; LC-TOF ($M+H^+$) calcd for $C_{35}H_{52}FN_4O_7$ 659.3820, found 659.3818.

5.2.4 (3*S*,4*S*)-*tert*-Butyl 3-((6-(bis(*tert*-butoxycarbonyl)amino)-4-methylpyridin-2-yl)methyl)-4-(2-(2-methoxybenzylamino)ethoxy)pyrrolidine-1-carboxylate (8b)—Compound **8b** was synthesized using a similar procedure to that of **8a** (88%): ^{1}H NMR (500 MHz, $CDCl_3$) 1.42–1.43 (s, 27H), 2.31–2.33 (m, 3H), 2.60–2.70 (m, 1H), 2.70–2.80 (m, 1H), 2.90–3.10 (m, 4H), 3.28–3.32 (m, 1H), 3.35–3.52 (m, 3H), 3.65–3.75 (m, 1H), 3.79–3.81 (m, 2H), 3.85–3.87 (m, 3H), 4.01–4.20 (m, 2H), 6.75–7.00 (m, 4H), 7.26–7.30 (m, 1H), 7.35–7.40 (m, 1H); ^{13}C NMR (125 MHz, $CDCl_3$) 20.9, 21.9, 27.9, 28.3, 28.4, 28.5, 29.7, 34.4, 34.5, 42.5, 43.2, 46.1, 47.5, 47.7, 48.7, 48.9, 50.3, 50.8, 55.4, 55.5, 55.6, 60.4, 65.2, 65.3, 79.3, 79.4, 79.8, 82.92, 82.94, 110.5, 110.6, 119.7, 119.8, 121.0, 121.2, 121.3, 122.7, 122.8, 130.50, 130.52, 131.4, 149.9, 151.47, 151.51, 151.77, 151.79, 154.5, 154.7, 157.7, 158.89, 158.91, 176.2; LC-TOF ($M+H^+$) calcd for $C_{36}H_{55}N_4O_8$ 671.4020, found 671.4016.

5.2.5 (3*S*,4*S*)-*tert*-Butyl 3-((6-(bis(*tert*-butoxycarbonyl)amino)-4-methylpyridin-2-yl)methyl)-4-(2-(2-hydroxybenzylamino)ethoxy)pyrrolidine-1-carboxylate (8c)—Compound **8c** was synthesized using a similar procedure to that of **8a** (55%): ^{1}H NMR (500 MHz, $CDCl_3$) 1.45–1.46 (s, 27H), 2.34 (s, 3H), 2.60–2.75 (m, 2H),

2.75–2.85 (m, 1H), 2.85–3.00 (m, 2H), 3.00–3.07 (m, 1H), 3.07–3.20 (m, 1H), 3.20–3.33 (m, 1H), 3.33–3.51 (m, 3H), 3.51–3.65 (m, 1H), 3.65–3.74 (m, 2H), 3.74–3.90 (m, 1H), 4.00–4.18 (m, 2H), 6.75–6.85 (m, 2H), 6.93 (s, 1H), 7.02–7.10 (m, 1H), 7.15–7.20 (m, 1H); ^{13}C NMR (125 MHz, $CDCl_3$) 20.9, 21.1, 27.9, 28.5, 29.7, 34.1, 42.4, 43.1, 46.8, 47.0, 48.4, 48.9, 50.1, 50.3, 50.7, 50.8, 53.4, 60.3, 66.3, 66.4, 78.6, 79.3, 79.5, 79.6, 82.9, 83.2, 83.3, 116.1, 116.3, 118.9, 119.4, 119.7, 120.3, 120.5, 120.9, 122.9, 123.0, 123.2, 128.8, 128.9, 129.4, 129.6, 129.7, 150.3, 150.6, 151.4, 151.6, 151.7, 154.7, 154.9, 157.2, 157.3, 159.1, 159.2; LC-TOF ($M+H^+$) calcd for $C_{35}H_{53}N_4O_8$ 657.3863, found 657.3874.

5.2.6 (3*S*,4*S*)-*tert*-Butyl 3-((6-(bis(*tert*-butoxycarbonyl)amino)-4-methylpyridin-2-yl)methyl)-4-(2-(furan-2-ylmethylamino)ethoxy)pyrrolidine-1-carboxylate(8d)—Compound **8b** was synthesized using a similar procedure to that of **8a** (90%): ^{1}H NMR (500 MHz, $CDCl_3$) 1.43–1.44 (s, 27H), 2.30–2.32 (m, 3H), 2.50–2.60 (m, 1H), 2.75–2.83 (m, 2H), 2.92–3.17 (m, 3H), 3.20–3.50 (m, 5H), 3.52–3.70 (m, 2H), 3.77–3.80 (m, 1H), 3.81 (s, 2H), 6.20–6.21 (d, J = 3.0 Hz, 1H), 6.32 (s, 1H), 6.86–6.92 (m, 2H), 7.37 (s, 1H); ^{13}C NMR (125 MHz, $CDCl_3$) 19.1, 20.9, 21.0, 23.4, 24.7, 27.9, 28.39, 28.48, 28.51, 29.7, 30.6, 34.6, 34.7, 36.6, 42.6, 43.2, 45.8, 45.9, 48.2, 48.3, 48.8, 49.1, 50.3, 50.8, 64.4, 68.2, 68.4, 78.7, 79.2, 79.3, 79.4, 82.85, 82.86, 107.0, 107.2, 110.16, 110.24, 119.57, 119.61, 122.8, 141.90, 141.94, 141.97, 149.6, 151.45, 151.50, 151.8, 153.4, 154.5, 154.7, 159.1, 159.2, 171.3; LC-TOF ($M+H^+$) calcd for $C_{33}H_{51}N_4O_8$ 631.3703, found 631.3703.

5.2.7 6-(((3*S*,4*S*)-4-(2-(2-Fluorobenzylamino)ethoxy)pyrrolidin-3-yl)methyl)-4-methylpyridin-2-amine (4a)—To a solution of **8a** (70 mg, 0.10 mmol) in MeOH (2 mL) was added 6 N HCl (4 mL) at room temperature. The mixture was stirred for 12 h and then concentrated. The crude product was purified by recrystallization ($EtOH/H_2O$) to give inhibitor **4a**(38 mg, 97%): ^{1}H NMR (500 MHz, D_2O) 2.18 (s, 3H), 2.68–2.73 (m, 1H), 2.76–2.82 (dd, J = 7.0, 15.5 Hz, 1H), 2.85–2.90 (dd, J = 8.0, 15.0 Hz, 1H), 3.04–3.09 (t, J = 11.5 Hz, 1H), 3.15–3.25 (m, 2H), 3.39–3.43 (dd, J = 8.5, 11.5 Hz, 1H), 3.50–3.53 (d, J = 13.5 Hz, 1H), 3.53–3.60 (m, 1H), 3.73–3.80 (m, 1H), 4.05–4.10 (m, 1H), 4.22 (s, 2H), 6.47 (s, 1H), 6.53 (s, 1H), 7.12–7.14 (dd, J = 1.0, 8.5 Hz, 1H), 7.16–7.18 (dd, J = 1.0, 8.0 Hz, 1H), 7.35–7.40 (m, 1H); ^{13}C NMR (125 MHz, D_2O) 21.0, 28.8, 41.3, 44.67, 44.70, 46.4, 47.1, 49.3, 63.9, 78.0, 110.3, 114.0, 115.8, 115.9, 117.4, 117.5, 125.0, 125.1, 132.1, 132.2, 132.3, 132.4, 145.7, 153.8, 158.1, 160.1, 162.0; LC-TOF ($M+H^+$) calcd for $C_{20}H_{28}FN_4O$ 359.2247, found 359.2253.

5.2.8 6-(((3*S*,4*S*)-4-(2-(2-Methoxybenzylamino)ethoxy)pyrrolidin-3-yl)methyl)-4-methylpyridin-2-amine (4b)—Compound **4b** was synthesized using a similar procedure to that of **4a** (96%): ^{1}H NMR (500 MHz, $CDCl_3$) 2.18 (s, 3H), 2.65–2.85 (m, 3H), 3.03–3.10 (t, J = 11.5 Hz, 1H), 3.17–3.32 (m, 3H), 3.40–3.47 (dd, J = 8.5, 12.0 Hz, 1H), 3.50–3.57 (m, 2H), 3.72–3.80 (m, 4H), 4.05–4.17 (m, 3H), 6.43 (s, 1H), 6.49 (s, 1H), 6.91–6.94 (dd, J = 7.0, 7.5 Hz, 1H), 6.97–6.99 (d, J = 8.5 Hz, 1H), 7.23–7.25 (dd, J = 1.0, 7.5 Hz, 1H), 7.34–7.38 (ddd, J = 1.5, 8.5, 9.0 Hz, 1H); ^{13}C NMR (125 MHz, $CDCl_3$) 21.0, 38.7, 41.0, 46.2, 46.9, 47.1, 49.1, 55.4, 64.0, 77.8, 110.3, 111.2, 113.8, 118.2, 121.0, 131.6, 131.8, 145.6, 153.8, 157.6, 158.0; LC-TOF ($M+H^+$) calcd for $C_{21}H_{31}N_4O_2$ 371.2447, found 371.2450.

5.2.9 2-((2-((3*S*,4*S*)-4-((6-Amino-4-methylpyridin-2-yl)methyl)pyrrolidin-3-yloxy)ethylamino)methyl)phenol (4c)—Compound **4c** was synthesized using a similar procedure to that of **4a** (92%): ^{1}H NMR (500 MHz, $CDCl_3$) 2.15 (s, 3H), 2.60–2.70 (m, 1H), 2.77–2.82 (m, 2H), 3.00–3.10 (t, J = 11.5 Hz, 1H), 3.18–3.22 (m, 3H), 3.42–3.51 (dd, J = 8.5, 11.5 Hz, 1H), 3.51–3.56 (m, 2H), 3.73–3.80 (m, 1H), 4.00–4.25 (m, 3H), 6.38 (s, 1H), 6.50 (s, 1H), 6.83–6.88 (m, 2H), 7.21–7.25 (m, 2H); ^{13}C NMR (125 MHz, $CDCl_3$) 21.0, 28.8, 41.2, 46.0, 47.0, 47.1, 49.2, 63.7, 77.8, 110.3, 114.0, 115.4, 117.0, 120.6, 131.6, 131.7,

145.6, 153.8, 155.0, 158.0; LC-TOF ($M+H^+$) calcd for $C_{20}H_{29}N_4O_2$ 357.2291, found 357.2277.

5.2.10 6-(((3*S*,4*S*)-4-(2-(Furan-2-ylmethylamino)ethoxy)pyrrolidin-3-yl)methyl)-4-methylpyridin-2-amine (4d)—Compound **4b** was synthesized using a similar procedure to that of **4a** (96%): ^{1}H NMR (500 MHz, $CDCl_3$) 2.32 (s, 3H), 2.65–2.73 (m, 1H), 2.76–2.83 (dd, *J* = 7.5, 15.0 Hz, 1H), 2.88–2.93 (dd, *J* = 7.5, 14.5 Hz, 1H), 3.04–3.09 (t, *J* =11.5 Hz, 1H), 3.17–3.24 (m, 3H), 3.39–3.43 (dd, *J* = 9.0, 11.5 Hz, 1H), 3.48–3.51 (d, *J* = 13.5 Hz, 2H), 3.51–3.56 (m, 1H), 3.70–3.75 (m, 1H), 4.05–4.10 (m, 1H), 4.22 (s, 2H), 6.38–6.40 (dd, *J* = 2.0, 5.0 Hz, 1H), 5.48 (s, 1H), 6.52–6.53 (d, *J* = 3.5 Hz, 1H), 6.55 (s, 1H),; ^{13}C NMR (125 MHz, $CDCl_3$) 21.0, 28.8, 41.4, 43.1, 46.0, 47.0, 49.4, 64.0, 78.1, 110.3, 110.8, 111.0, 113.0, 114.0, 144.1, 144.3, 144.9, 145.8, 153.9, 158.1; LC-TOF ($M+H^+$) calcd for $C_{18}H_{27}N_4O_2$ 331.2134, found 331.2136.

5.3 NOS Purified Enzyme Assays

The three NOS isoforms, rat nNOS, murine iNOS, and bovine eNOS were obtained as recombinant enzymes overexpressed in and purified from *E. coli* as previously reported.[36–39] The hemoglobin capture assay was used to measure nitric oxide production.[40] Briefly, the assay was run at 37 °C in 100 mM HEPES buffer (10% glycerol; pH 7.4) in the presence of 10 μM L-arginine. The following were also included in the assay: 100 μM NADPH, 10 μM tetrahydrobiopterin, 1 mM $CaCl_2$, 11.6 μg/mL calmodulin and 3.0 μM oxyhemoglobin. For iNOS, calmodulin and $CaCl_2$ were omitted because iNOS is calcium independent; CaM is bound tightly. All NOS isozymes were used at a concentration of approximately 100 nM. The assay was run in a 96 well plate, using the Synergy 4 by BioTek, at the Northwestern University High Throughput Analysis Facility. The assay was run in triplicate; Forty-eight 100 μL reactions were performed at once. The addition of hemoglobin and NOS were automated with a maximum of a 30 second delay before the reactions could be recorded at 401 nm. The absorbance increase at 401 nm is due to the formation of NO via the conversion of oxyhemoglobin to methemoglobin, The IC_{50} values were obtained using non-linear regression in GraphPad Prism5 software. Subsequent K_i values were determined using the Cheng-Prusoff relationship:[41]

$$K_i = IC_{50}/(1+[S]/K_m)$$

The following known K_m values were used: rat nNOS 1.3 μM; murine iNOS 8.3 μM; bovine eNOS 1.7 μM.

5.4 nNOS Cell-Based Assay

HEK293t cells stably transfected with rat nNOS were cultured as previously described.[28] The nNOS inhibition assay was performed as previously reported,[28] with the following modifications: assays were performed in 96-well plates with a total volume of 100 μL, and 10 μM A23187 (Sigma Aldrich, St Louis, MO, USA) (added as 100x stock in 50% DMSO) was used in place of 5 μM. A23187 is a calcium ionophore; it transports calcium into the cells and activates nNOS. Nine concentrations of each inhibitor were tested, in at least triplicate wells. All inhibitors were assayed within the same experiment to assure consistencies in cell concentration and passage number. The entire assay was repeated at least three times for each inhibitor, and the IC_{50} values averaged. Cells were plated in the 96-well plates 24 hours before activation. After 6 hours of activation (in the presence or absence of inhibitor, which was added 30 minutes before activation) 50 μL aliquots of the media were removed and nitrite production was quantified using Griess reagent.[35]

5.5 Crystal Preparation, X-ray Diffraction Data Collection, and Structure Refinement

The nNOS heme domain protein used for crystallization was generated by limited trypsin digest from the full length nNOS and further purified through a Superdex 200 gel filtration column (GE Healthcare) as described previously.[42] The nNOS heme domain at 7–9 mg/mL containing 20 mM histidine was used for the sitting drop vapor diffusion crystallization setup under the conditions reported [42] with minor modification by addition of 10% (v/v) ethylene glycol in well solution. Fresh crystals were first passed stepwise through cryo-protectant solutions as described [42] and then soaked with 10 mM inhibitor for 4–6 h at 4 °C before being flash cooled by plunging into liquid nitrogen.

The cryogenic (100K) X-ray diffraction data were collected remotely at beamline 7-1 at Stanford Synchrotron Radiation Light source through the data collection control software Blu-Ice [43] and the crystal mounting robot. Raw data frames were indexed, integrated, and scaled using HKL2000.[44] The binding of inhibitors was detected by the initial difference Fourier maps calculated with REFMAC.[45] The inhibitor molecules were then modeled in COOT [46] and refined using REFMAC. Water molecules were added in REFMAC and checked by COOT. The TLS [47] protocol was implemented in the final stage of refinements with each subunit as one TLS group. The refined structures were validated in COOT before deposition to RCSB protein data bank. The crystallographic data collection and structure refinement statistics are summarized in Table 3 with PDB accession codes included.

Supplementary Material

Refer to Web version on PubMed Central for supplementary material.

Acknowledgments

We are grateful to the National Institutes of Health, Grants GM049725 to RBS and GM057353 to TLP. We thank Dr. Bettie Sue Siler Masters (NIH grant GM52419, with whose laboratory P.M. and L.J.R. are affiliated). B.S.S.M. also is grateful to the Welch Foundation for a Robert A. Welch Distinguished Professorship in Chemistry (AQ0012). P.M. is supported by grant 0021620849from MSMT of the Czech Republic. We thank the SSRL beamline staff for their support during remote X-ray diffraction data collection. We thank Drs. Josh Kurutz and Yuyang Wu of the Northwestern University IMSERC facility for valuable assistance and discussions concerning the NMR experiments.

Abbreviations

CNS	central nervous system
NO	nitric oxide
nNOS	neuronal nitric oxide synthase
eNOS	endothelial nitric oxide synthase
iNOS	inducible nitric oxide synthase
BBB	blood brain barrier
H-bond	hydrogen bond
L-NNA	L -N-nitroarginine
H_4B	tetrahydrobiopterin

References

1. Dorheim MA, Tracey WR, Pollock JS, Grammas P. Biochem Biophys Res Commun. 1994; 205:659–665. [PubMed: 7528015]
2. Zhang L, Dawson VL, Dawson TM. Pharmacol Ther. 2006; 109:33–41. [PubMed: 16005074]
3. Norris PJ, Waldvogel HJ, Faull RLM, Love DR, Emson PC. Neuroscience. 1996; 72:1037–1047. [PubMed: 8735228]
4. Ashina M. Expert Opin Pharmacother. 2002; 3:395–399. [PubMed: 11934342]
5. Sims NR, Anderson MF. Neurochem Int. 2002; 40:511–526. [PubMed: 11850108]
6. Southan GJ, Szabó C. Biochem Pharmacol. 1996; 51:383–394. [PubMed: 8619882]
7. Babu BR, Griffith OW. Curr Opin Chem Biol. 1998; 2:491–500. [PubMed: 9736922]
8. Alderton WK, Cooper CE, Knowles RG. Biochem J. 2001; 357:593–615. [PubMed: 11463332]
9. Ji, H.; Erdal, E.; Litzinger, EA.; Seo, J.; Zhu, Y.; Xue, F.; Fang, J.; Huang, J.; Silverman, RB. Frontiers in Medicinal Chemistry. 5. Reitz, AB.; Choudhary, MI.; Atta-ur-Rahman, editors. Bentham Science Publishers; 2009. p. 842-882.
10. Silverman RB. Acc Chem Res. 2009; 42:439–451. [PubMed: 19154146]
11. Delker SL, Ji H, Li H, Jamal J, Fang J, Xue F, Silverman RB, Poulos TL. J Am Chem Soc. 2010; 132:5437–5442. [PubMed: 20337441]
12. Ji H, Tan S, Igarashi J, Li H, Derrick M, Martásek P, Roman LJ, Vásquez-Vivar J, Poulos TL, Silverman RB. Ann Neurol. 2009; 65:209–217. [PubMed: 19235180]
13. Lawton GR, Ralay Ranaivo H, Chico LK, Ji H, Xue F, Martásek P, Roman LJ, Watterson DM, Silverman RB. Bioorg Med Chem. 2009; 17:2371–2380. [PubMed: 19268602]
14. Xue F, Fang J, Lewis WW, Martásek P, Roman LJ, Silverman RB. Bioorg Med Chem Lett. 2010; 20:554–557. [PubMed: 19963381]
15. Xue F, Huang J, Ji H, Fang J, Li H, Martásek P, Roman LJ, Poulos TL, Silverman RB. Bioorg Med Chem. 2010; 18:6526–6537. [PubMed: 20673724]
16. Xue F, Li H, Fang J, Roman LJ, Martásek P, Poulos TL, Silverman RB. Bioorg Med Chem Lett. 2010; 20:6258–6261. [PubMed: 20833542]
17. Xue F, Li H, Delker SL, Fang J, Martásek P, Roman LJ, Poulos TL, Silverman RB. J Am Chem Soc. 2010; 132:14229–14238. [PubMed: 20843082]
18. Kuhn B, Mohr P, Stahl M. J Med Chem. 2010; 53:2601–2611. [PubMed: 20175530]
19. Laurence C, Brameld KA, Graton J, Le Questel JY, Renault E. J Med Chem. 2009; 52:4073–4086. [PubMed: 19537797]
20. Jansma A, Zhang Q, Li B, Ding Q, Uno T, Bursulaya B, Liu Y, Furet P, Gray NS, Geierstanger BH. J Med Chem. 2007; 50:5875–5877. [PubMed: 17975906]
21. McDonagh AF, Lightner DA. J Med Chem. 2007; 50:480–488. [PubMed: 17266200]
22. Sasaki S, Cho N, Nara Y, Harada M, Endo S, Suzuki N, Furuya S, Fujino M. J Med Chem. 2003; 46:113–124. [PubMed: 12502365]
23. Alex A, Millan DS, Perez M, Wakenhut F, Whitlock GA. Med Chem Commun. 2011; 2:669–674.
24. Ashwood VA, Field MJ, Horwell DC, Julien-Larose C, Lewthwaite RA, McCleary S, Pritchard MC, Raphy J, Singh L. J Med Chem. 2001; 44:2276–2285. [PubMed: 11428921]
25. Ji H, Li H, Martásek P, Roman LJ, Poulos TL, Silverman RB. J Med Chem. 2009; 52:779–797. [PubMed: 19125620]
26. Ji H, Delker SL, Li H, Martásek P, Roman LJ, Poulos TL, Silverman RB. J Med Chem. 2010; 53:7804–7824. [PubMed: 20958055]
27. Xue F, Kraus JM, Labby KJ, Ji H, Mataka J, Xia G, Li H, Delker SL, Roman LJ, Martásek P, Poulos TL, Silverman RB. J Med Chem. 2011; 54:6399–6403. [PubMed: 21809851]
28. Haight AR, Stoner EJ, Peterson MJ, Grover VK. J Org Chem. 2003; 68:8092–8096. [PubMed: 14535788]
29. Fang J, Silverman RB. Anal Biochem. 2009; 390:74–78. [PubMed: 19362065]
30. Viswanadhan VN, Ghose AK, Revankar GR, Robins RK. J Che Inf Comput Sci. 1989; 29:163–172.

31. Oki M. Top Stereochem. 1983; 14:1–81.
32. Clayden J, Moran WJ, Edwards PJ, LaPlante SR. Angew Chem Int Ed. 2009; 48:6398–6401.
33. Kraus JM, Tatipaka HB, McGuffin SA, Chennamaneni NK, Karimi M, Arif J, Verlinde CLMJ, Buckner FS, Gelb MH. J Med Chem. 2010; 53:3887–3898. [PubMed: 20429511]
34. Wilson JC, Munro SLA, Craik DJ. Magn Reson Chem. 1995; 33:367–374.
35. Ballet S, Misicka A, Kosson P, Lemieux C, Chung NN, Schiller PW, Lipkowski AW, Tourwé D. J Med Chem. 2008; 51:2571–2574. [PubMed: 18370374]
36. Hevel JM, White KA, Marletta MA. J Biol Chem. 1991; 266:22789–22791. [PubMed: 1720773]
37. Roman LJ, Sheta EA, Martasek P, Gross SS, Liu Q, Masters BS. Proc Natl Acad Sci USa. 1995; 92:8428–8432. [PubMed: 7545302]
38. Gerber NC, Ortiz de Montellano PR. J Biol Chem. 1995; 270:17791–17796. [PubMed: 7543092]
39. Martasek P, Liu Q, Liu J, Roman L, Gross S. Biochem Biophys Res Comm. 1996
40. Hevel JM, Marletta MA. Methods Enzymol. 1994; 233:250–258. [PubMed: 7516999]
41. Cheng YC, Prusoff WH. Biochem Pharmacol. 1973; 22:3099–3108. [PubMed: 4202581]
42. Li H, Shimizu H, Flinspach M, Jamal J, Yang W, Xian M, Cai T, Wen EZ, Jia Q, Wang PG, Poulos TL. Biochemistry. 2002; 41:13868–13875. [PubMed: 12437343]
43. McPhillips TM, McPhillips SE, Chiu HJ, Cohen AE, Deacon AM, Ellis PJ, Garman E, Gonzalez A, Sauter NK, Phizackerley RP, Soltis SM, Kuhn P. J Synchrotron Radiat. 2002; 9:401–406. [PubMed: 12409628]
44. Otwinowski Z, Minor W. Methods Enzymol. 1997; 276:307–326.
45. Murshudov GN, Vagin AA, Dodson EJ. Acta Crystallogr, Sect D: Biol Crystallogr. 1997; 53:240–255. [PubMed: 15299926]
46. Emsley P, Cowtan K. Acta Crystallogr, Sect D: Biol Crystallogr. 2004; D60:2126–2132. [PubMed: 15572765]
47. Winn MD, Isupov MN, Murshudov GN. Acta Crystallogr, Sect D: Biol Crystallogr. 2001; D57:122–133. [PubMed: 11134934]

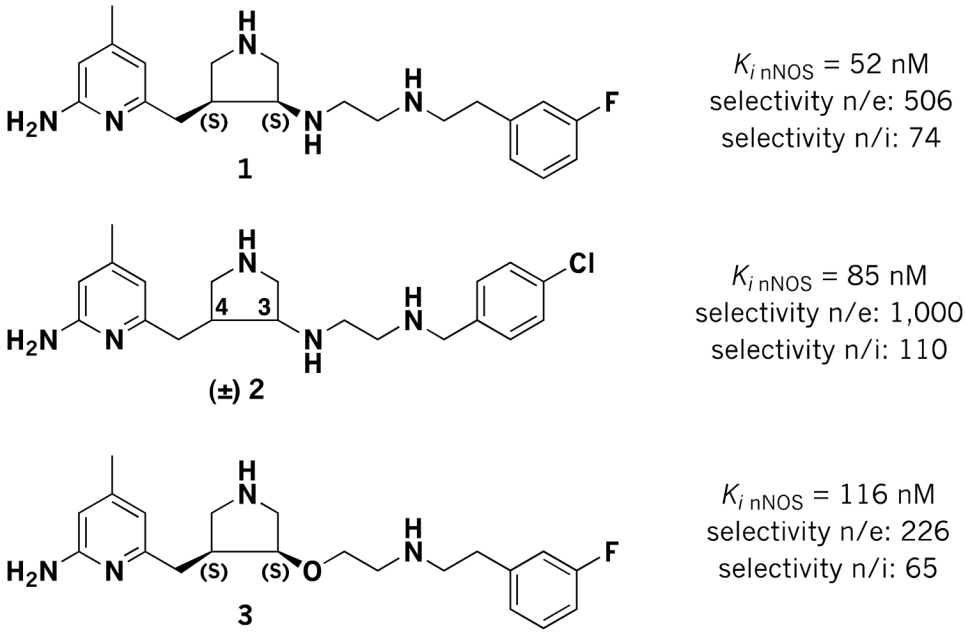

Figure 1.
Chemical structures and inhibitory activities of inhibitors (3*S,4S*)-**1** and (3*S,4S*)-**3** and (±)-**2**.

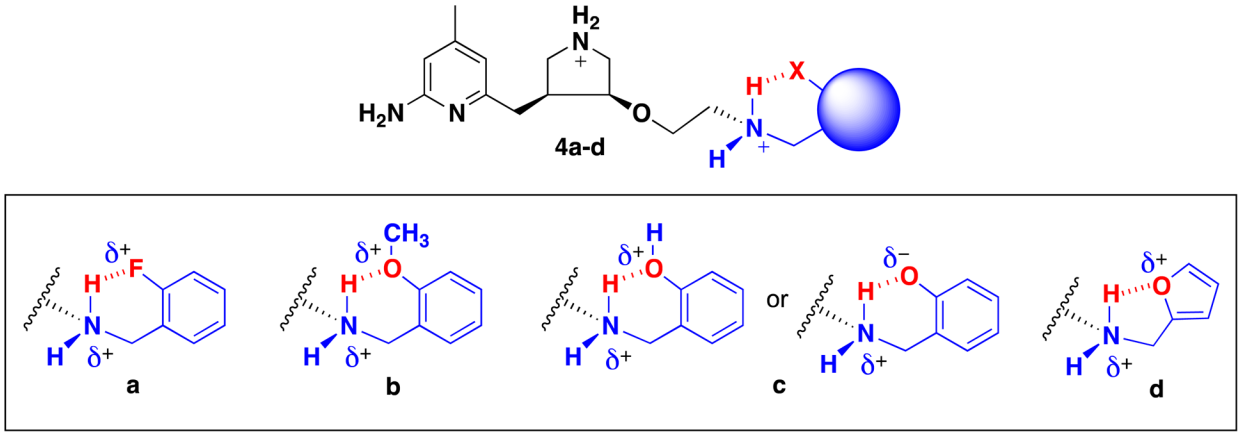

Figure 2.

Chemical structures of (*S.S*)-**4a**–**d**. The desired hydrogen bond is shown in red. Inhibitor **4c** may take on a conformation in which the −OH acts as both a H-bond acceptor and donor, delocalizing the positively charged nitrogen.

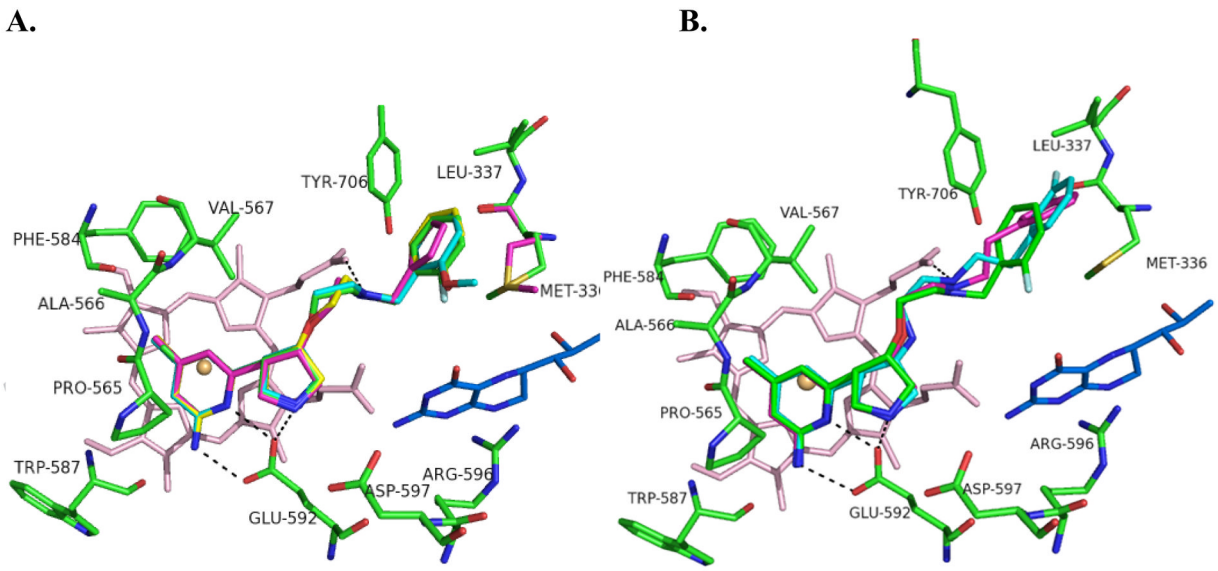

Figure 3.

A. Binding conformations of **4a–4d** overlaid: **4a** (green), **4b** (cyan), **4c** (yellow), **4d** (magenta); heme is shown in light pink; H_4B (tetrahydrobiopterin) is blue. The enzyme conformation is highly conserved between all four structures; therefore only the active site residues from the crystal structure of **4a** are shown. Met336 of the **4d** crystal structure is also shown (magenta) because of the difference in its configuration. **B**. Binding conformations of **1** (3JWS, cyan), **3** (3NLK, magenta) and **4a** (green), overlaid. Residues overlay almost exactly; therefore only those corresponding to the crystal structure of **4a** are shown. Hydrogen bonds are depicted with dashed lines. PDB codes: nNOS-**4a**, 3TYL; nNOS-**4b**, 3TYM; nNOS-**4c**, 3TYN; nNOS-**4d**, 3TYO.

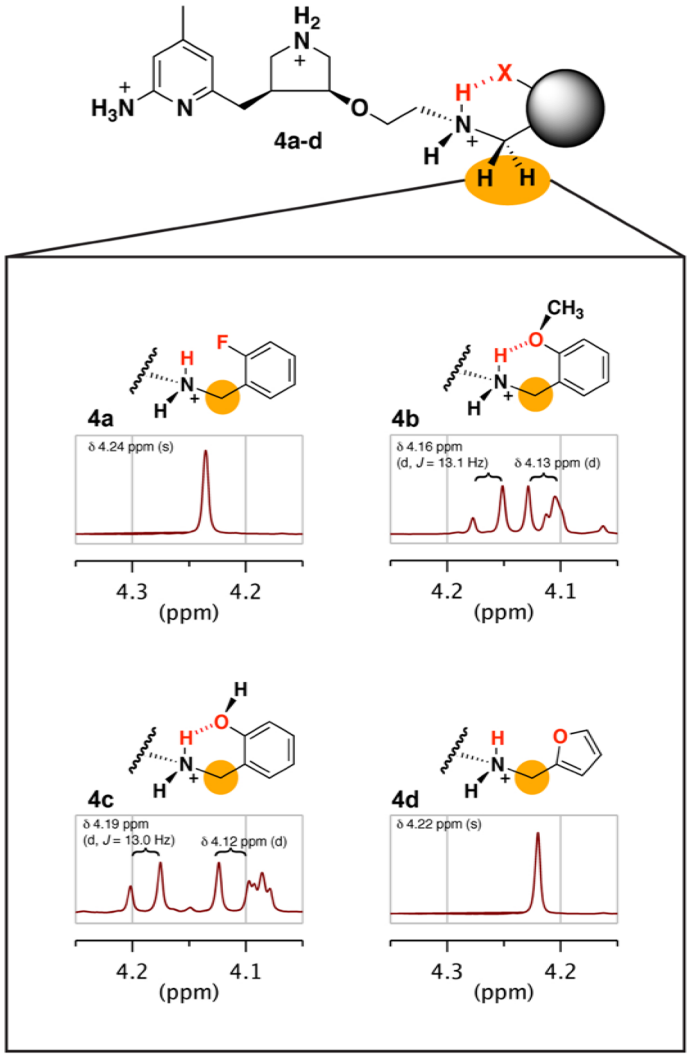

Figure 4.

^{1}H NMR spectra of **4a–4d** taken in D_2O at 25 °C. Doublets appear in place of the singlet usually seen with compounds of this scaffold for the methylene protons adjacent to the H-bondedamine in **4b** and **4c**; this is evidence for the H-bond. In both cases, the doublet further upfield overlaps with the triplet from one of the pyrrolidine hydrogens; a coupling value cannot be reported for the doublet further upfield but is presumed to be the same.

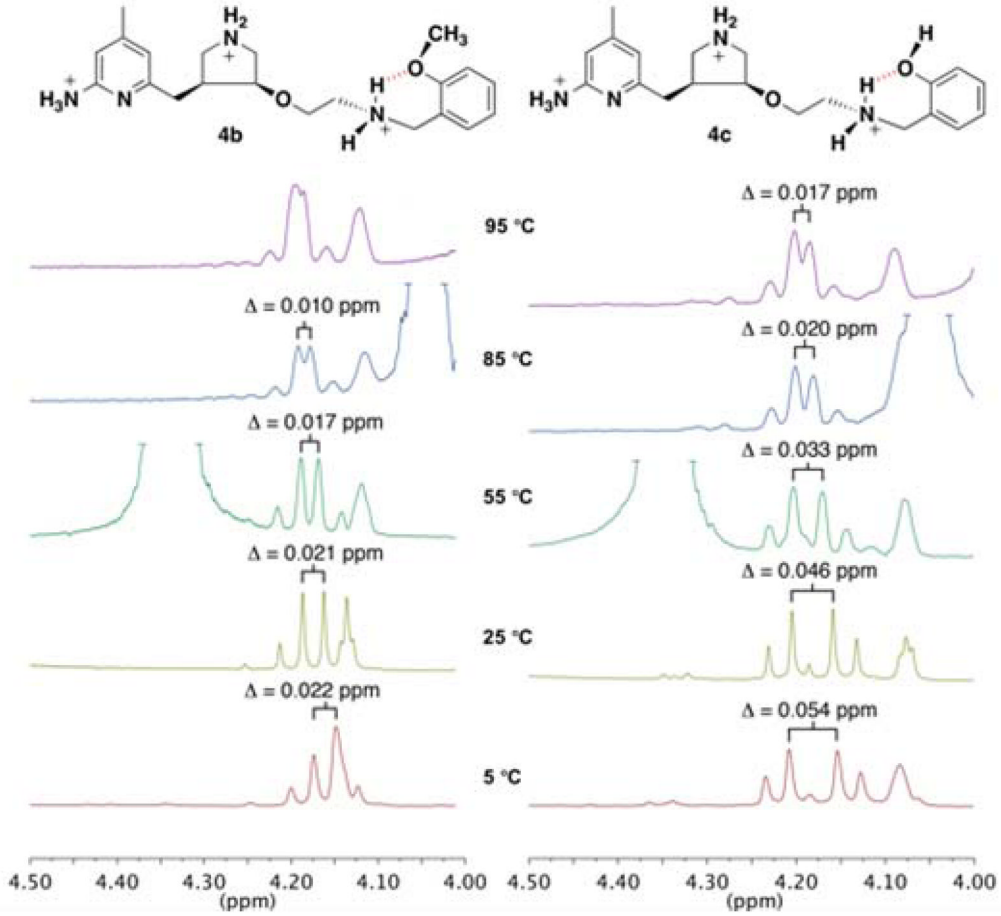

Figure 5.

^{1}H NMR spectra of **4b** and **4c** in D_2O at 95, 85, 55, 25, and 5 °C. The AB doublets shift toward one another at higher temperatures. In the spectra of **4b**, the doublet further upfield is obscured by the shift of a pyrrolidine proton (4.12 at 25 °C). The *J* value within the doublets remains the same, *J* = ~13 Hz. The difference between the chemical shifts ( ) is reported to better illustrate the changes in the chemical shifts, as instrument resolution is lost at higher temperatures.

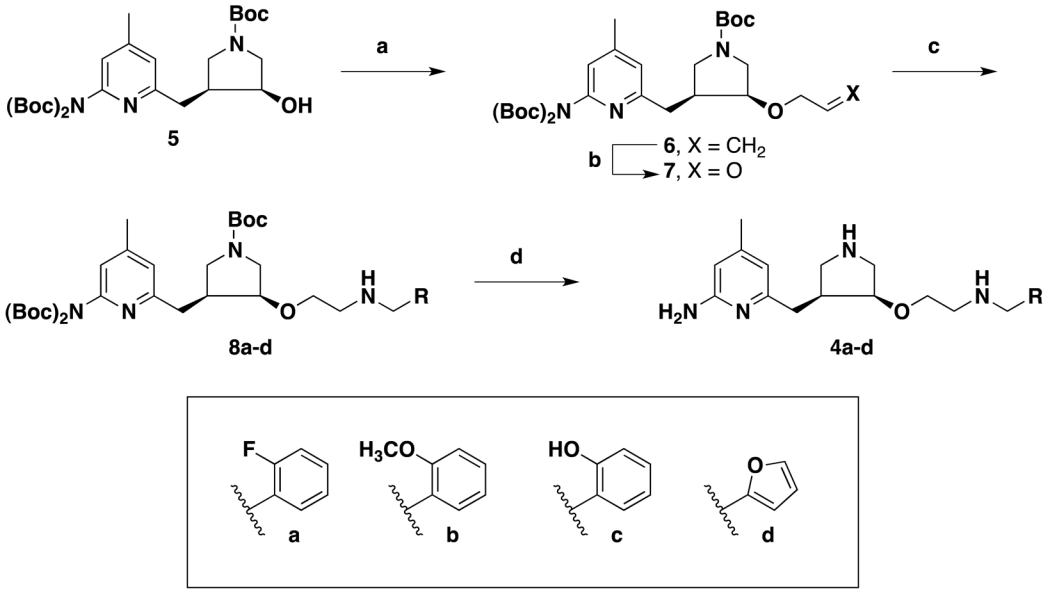

Scheme 1.

Synthesis of **4a**–**d**.

Reagents and conditions: (a) allyl methyl carbonate, $Pd(PPh_3)_4$, 45 °C, 5 h, 66%; (b) O_3, −78 °C, 30 min, (ii) Me_2S, −78 °C to rt, 2 h, 87%; (c) amines, $NaHB(OAc)_3$, rt, 3 h, 91%; (d) 6 N HCl in MeOH (2:1), rt, 12 h, 99%.

Table 1

K_i [a] values of **1**–**3** and **4a**–**4d** with all three NOS isoforms.

				selectivity[b]	
Compound	**nNOS (μM)**	**eNOS (μM)**	**iNOS (μM)**	**n/e**	**n/i**
1[c]	0.052	26	3.9	505	74
2[d]	0.085	85	9.4	1000	110
3[c]	0.12	26	7.5	226	65
4a	0.41	40	44	98	105
4b	0.82	77	114	93	139
4c	0.39	37	57	93	143
4d	0.40	66	36	169	92

[a] The K_i values were calculated based on the directly measured IC_{50} values (see methods), which represent at least triplicate measurements with standard deviations of ±10%.

[b] The ratio of K_i (eNOS or iNOS) to K_i (nNOS).

[c] Data from reference 26.

[d] Data from reference 25.

Table 2

IC_{50} values[a] of NOS inhibitors in purified enzyme assay and cell-based assay. See methods for assay details.

Compound	Purified IC_{50} (μM)	Cell-based IC_{50} (μM)	Relative Permeability Index (RPI)[b] (Cell based IC_{50}/Purified IC_{50})
1	0.45	19	42
2	0.74	42	57
3	1.0	13	13
4a	3.6	11	3.1
4b	7.1	22	3.1
4c	3.5	43	12
4d	3.4	100	29
aminopyridine[c]	0.05	25	500
L-NNA[d]	5.0	5.0	1

[a] See methods. IC_{50} values represent at least triplicate measurements with standard deviations of less than10%.

[b] The smaller the number, the closer the difference in IC_{50} for the cell-based assay and purified enzyme assay, which suggests improved permeability into cells.

[c] aminopyridine = 2-amino-4,6-dimethylpyridine hydrochloride.

[d] L-NNA = L-*N*-nitroarginine.

Table 3

Crystallographic data collection and refinement statistics

Data set[a]	nNOS-4a	nNOS-4b	nNOS-4c	nNOS-4d
PDB code	3TYL	3TYM	3TYN	3TYO
Data collection				
Space group	$P2_12_12_1$	$P2_12_12_1$	$P2_12_12_1$	$P2_12_12_1$
Cell dimensions				
a, *b*, *c* (Å)	51.9, 110.8, 164.3	51.8, 110.7, 164.2	51.8, 110.8, 164.2	51.9, 110.9, 164.3
Resolution (Å)	1.90 (1.93-1.90)	2.00 (2.03-2.00)	1.97 (2.00-1.97)	1.93 (1.96-1.93)
R_{sym} or R_{merge}	0.055 (0.629)	0.056 (0.590)	0.046 (0.564)	0.047 (0.605)
I/σ	29.2 (2.1)	15.6 (2.0)	31.0 (2.5)	32.1 (2.5)
No. unique reflections	75,516	64,550	67,186	72,491
Completeness (%)	99.9 (100.0)	99.9 (97.8)	98.8 (98.0)	99.8 (99.9)
Redundancy	4.1 (4.1)	4.1 (4.1)	4.1 (4.1)	4.1 (4.0)
Refinement				
Resolution (Å)	1.90	2.00	1.97	1.93
No. reflections	71,520	61,119	63,641	68,646
R_{work}/R_{free}[2]	0.179/0.212	0.186/0.227	0.185/0.223	0.180/0.215
No. atoms				
Protein	6709	6671	6679	6671
Ligand/ion	185	183	181	177
Water	377	283	321	366
Mean *B*-factor	45.16	49.50	48.17	47.50
R.m.s. deviations				
Bond lengths (Å)	0.014	0.013	0.013	0.012
Bond angles (°)	1.411	1.386	1.403	1.324

[a] See Figure 1 for chemical formula of inhibitors.